

Numerical Simulation of Faraday Probe Measurements in a Multi-component Non-equilibrium Plasma

IEPC-2005-85

Presented at the 29th International Electric Propulsion Conference, Princeton University,
October 31 – November 4, 2005

Jeremiah J. Boerner* and Iain D. Boyd†

Department of Aerospace Engineering, University of Michigan, Ann Arbor, MI, 48109

Abstract: This study investigates the axisymmetric plasma flow field near a Faraday probe. A hybrid computational code simulates electrons with a fluid model using the Boltzmann relation, and heavy particles with a Particle In Cell method. The planar Bohm sheath solution is shown to be a reliable predictor for a two-component beam and charge exchange plasma, representative of a low-power Hall thruster plume. Configurations with guard ring bias set to potentials ± 5 V from the collecting surface cause a small focusing effect, altering the collected current by 10% or less. A partial Langmuir probe characteristic from -10 V to 0 V shows excellent agreement with theoretical values for both ion and electron currents.

Nomenclature

e	=	electron charge
ϵ_0	=	permittivity of free space
k_B	=	Boltzmann constant
L_D	=	Debye length
M	=	Mach number with respect to Bohm velocity
m_i	=	ion mass
n_e	=	electron number density
n_i	=	ion number density
Φ	=	local potential
T_e	=	electron temperature
T_i	=	ion temperature
u_i	=	ion velocity
v_B	=	Bohm velocity
v_i	=	ion drift velocity
x	=	sheath coordinate

I. Introduction

CONTINUING development of next-generation Hall thrusters and ion engines includes life tests, performance evaluation, and spacecraft integration. One important concern in the use of EP thrusters is the impingement of high-energy ions on spacecraft surfaces, leading to material erosion or deposition. Measurements of plasma properties in the exhaust plume are used to evaluate thruster performance and characterize the operating conditions. Common experimental diagnostics include the Faraday probe, Langmuir probe, and Retarding Potential Analyzer (RPA).¹⁻³ Each of these instruments is immersed in the exhaust plume and may affect the plasma with both physical obstruction and electrostatic sheaths, making it difficult to recover undisturbed conditions from the measurements.

* Graduate Student, Aerospace Engineering (jboerner@umich.edu).

† Professor, Aerospace Engineering (iainboyd@umich.edu).

This paper compares the results of numerical simulation of a Faraday probe with electrostatic Bohm sheath theory. The planar Bohm sheath solution is outlined in a non-dimensional form. The computational code is briefly introduced along with a description of the ion distributions and probe geometry used in this work. Computational flow fields near a uniform potential probe are presented to establish the validity of the Bohm sheath solution. The focusing effect of a guard ring biased at a different potential from the collecting surface is investigated in terms of the collected current. Lastly, a simulated current-voltage (IV) characteristic is presented for the probe.

II. Planar Bohm Sheath Solution

Electrostatic probes are simple, inexpensive diagnostics that are widely used to measure a number of plasma parameters. A Faraday cup can be reduced to a current collecting surface, often negatively biased to repel electrons, which measures ion current. The most basic Langmuir probe is little more than a wire inserted into a plasma. Electron temperature, plasma potential, floating potential, and number density can all be determined from a record of collected current over a range of bias voltage.

The presence of a fixed-potential surface in the plasma necessitates the formation of a sheath. The sheath structure is often divided as in Fig. 1, featuring undisturbed neutral plasma far from the surface, an approximately neutral presheath region with small potential gradient, and a non-neutral sheath region with large potential gradient within a few Debye lengths of the surface.

For a collisionless planar sheath with cold ions, continuity and conservation of energy for the ions can be expressed in terms of the ion density, n_i , and velocity, u_i , as

$$n_i(x)u_i(x) = n_{is}u_{is} \quad (1)$$

$$\frac{1}{2}m_i u_i^2(x) + e\phi(x) = \frac{1}{2}m_i u_{is}^2 \quad (2)$$

where the subscript s refers to values at the edge of the sheath. The sheath edge ($x = 0$) is properly defined as the point where the electron and ion number densities are equal.

For a steady sheath, the electrons assume a Maxwellian distribution. The electron number density is then determined from the local potential through the Boltzmann relation.

$$n_e(x) = n_{is} \exp\left(\frac{e\phi(x)}{k_B T_e}\right) \quad (3)$$

Poisson's equation closes the set by relating the potential to the ion and electron number densities in the sheath.

$$\frac{d^2\phi(x)}{dx^2} = -\frac{e}{\epsilon_0}(n_i(x) - n_e(x)) \quad (4)$$

A second-order differential equation for the potential is obtained when Eqs. (1)-(3) are used to eliminate u_i and combined into Eq. (4). Normalizing the potential by the electron temperature suggests the Debye length, L_D , and Bohm velocity, v_B , as appropriate length and velocity scales. The Mach number based on Bohm velocity, M , is the sole parameter remaining after this process.^{4,5} The plasma is assumed to have zero potential and no electric field (zero potential gradient) at the sheath edge, providing the necessary boundary conditions for integration.

The first integration can be performed analytically to yield Eq. (5), but the second integration must be performed numerically. Ion and electron properties are then easily recovered using the preceding relations.

$$\frac{1}{2}\left(\frac{d\Phi}{dz}\right)^2 = \exp(-\Phi) - 1 - M^2 \left[\left(1 + \frac{2}{M^2}\Phi\right)^{\frac{1}{2}} - 1 \right] \quad (5)$$

A Taylor expansion about $z = 0$ of this intermediate result shows that $M^2 > 1$ is required for the solution to be steady. That is, ions must enter the sheath edge at the Bohm velocity or faster to develop a stable sheath. Ions in the exhaust plume of EP devices are typically supersonic so this condition is easily satisfied. In other applications where the ions are slow moving or stationary, a presheath structure must form to accelerate ions up to the Bohm velocity at the sheath edge.

III. Model Description

Our computational model simulates 2D axisymmetric flow using a hybrid Particle In Cell (PIC) method. Ions and neutrals are treated with a PIC model, while electrons are simulated with a fluid model.⁶ The cylindrical Faraday probe geometry lends itself to a computational grid consisting of equally spaced rectangular cells.

Ions and neutrals are simulated with the PIC module. Particle weights (the number of real atoms represented by a simulated particle) are varied in steps from the centerline to the outer edge of the domain. This limits the number of simulated particles, thereby reducing the total computation time. Macroscopic properties are determined from weighted averages of the particles within a cell. A self-consistent potential field is calculated from Poisson's equation using an Alternating Direction Implicit (ADI) solver. Electrostatic fields are then calculated from the gradient of the potential and applied to the particles. A Direct Simulation Monte Carlo (DSMC) routine⁷ is in place to handle collisions, although the plasma conditions in this study are very nearly collisionless.

Two models are available for simulating the electron fluid. The first is a detailed fluid model that explicitly tracks electron continuity, momentum, and energy. The second is a simplified Boltzmann model where a streamfunction is used instead of the continuity equation, and the Boltzmann relation is used in place of the momentum equation. Comparisons of preliminary results from both models show only negligible differences and confirm that the electrons remain isothermal. Since the Bohm sheath solution assumes that electrons follow the Boltzmann relation, the Boltzmann model is used for the results that follow.

The computational domain is shown schematically in Fig. 2, with the probe front surface divided into collecting region and guard ring. Most experimental configurations apply a single potential on the entire probe with the goal of producing a uniform sheath over the collecting surface. The computational code allows collecting surface and guard ring biases to be set separately. Values for potential and electron streamfunction are assigned along these edges.

Ion particles undergo diffuse reflection and are converted to neutral particles at probe surfaces. Charged particle collisions with the collecting surface are recorded and weighted by the area of the impacted edge. A sum over the weighted current bits gives the total collected current. The collected ion and electron currents are averaged during the sampling process along with other macroscopic properties.

At the upstream edge, an inlet boundary generates the ion particles that enter the domain during a time step. The velocity of each particle is selected from a Maxwellian distribution using an acceptance/rejection method, with ion thermal temperature and drift velocity included as inputs. For simulations with more than one ion population, each component of the distribution is sampled separately. Gradients of potential and electron streamfunction are specified along this edge. The outer radial edge likewise has an inlet boundary condition and introduces particles from the same distributions as the upstream inlet. Radial gradients in electron properties are set to zero along this edge.

IV. Effects of Upstream Plasma Distribution

Although elementary probe theory only accounts for an isothermal ion distribution, the Bohm sheath solution remains a good predictor when applied to a Maxwellian ion distribution.⁸ A more accurate EP plume distribution includes both a high-temperature high-velocity beam population and a low-temperature low-velocity charge exchange (CEX) population. Both of these distributions are considered in this section, with emphasis on any differences in the ion current collected by the probe.

Undisturbed plasma properties are representative of the flow downstream of an EP thruster. In particular, we choose values from 50 cm downstream and 75° off-axis in the exhaust plume of a Busek Co. "BHT-200" 200 W xenon Hall thruster. This is a region of interest since experimental measurements suggest that the majority of the ion flux is due to CEX ions; that is, low-energy ions formed by collisions downstream of the thruster's acceleration region. This low-energy population may be focused by electric fields near the probe and lead to an over-estimate of the ion current. Calculations that rely on the measured current, such as integrated discharge current, will be skewed accordingly.

Previous numerical simulations of the BHT-200 flow field provide the Maxwellian distribution properties listed in the first column of Table 1 as “single beam.”⁹ Experimental Langmuir probe measurements taken by Ma at the same location give similar magnitude values for ion number density and electron temperature.¹⁰ In that experimental setup, the Faraday probe is biased to -5 V to repel electrons.

A more realistic distribution consists of two superimposed Maxwellian distributions. The first distribution is simply the beam ions, with the same temperature and drift velocity as before. The second distribution describes the CEX ions, with much lower temperature and drift velocity. Relative densities for the two populations are selected to reproduce the difference in collected current measured by a collimated probe (only beam ions) versus an uncollimated probe (both beam and CEX ions) at 60 cm downstream and 75° off-axis in the plume of a BPT-4000 Hall thruster.¹¹ Total density is selected such that the current flux for this distribution remains equal to that of the single beam Maxwellian distribution. These distribution properties are recorded in Table 1 as “composite beam” and “composite CEX.” The single beam distribution and the composite total distribution are shown together in Fig. 3 for comparison.

Table 1. Distribution properties for a Maxwellian beam population and a composite beam-CEX population in a simulated BHT-200 plume.

	Single Beam	Composite		
		Beam	CEX	Bulk
$n_i, 10^{14} \text{ m}^{-3}$	1.100	0.4795	1.439	1.919
$v_i, \text{ m/s}$	2,381	2,381	1,026	1,365
$T_i, \text{ K}$	11,600	11,600	300	—
$L_D, 10^{-4} \text{ m}$	7.09	10.74	6.20	5.37
$v_B, \text{ m/s}$	855.3	855.3	855.3	855.3
M	2.78	2.78	1.20	1.60

The Bohm sheath solution is obtained for each of the component distributions using the approach outlined previously. Due to its low freestream drift velocity, the composite CEX ion distribution develops the longest sheath. Figures 4-6, respectively, show normalized profiles of potential, electron number density, and ion number density in that sheath. Plasma potential decays to 1% of the bias value by $9L_D$ from the probe surface. Ion and electron number density are affected over a longer distance, approaching within 1% of the undisturbed values at $12L_D$ from the probe.

As a note to interpreting these figures, ion flux is conserved throughout the sheath but electron flux is not. Therefore, the decrease of ion density depicted in Fig. 6 indicates an increase in velocity. In contrast, the decrease in electron density in Fig. 5 corresponds to the smaller fraction of the distribution with initial kinetic energy sufficient to reach the local potential.

The Bohm sheath solution provides an estimate of the required domain length, suggesting an upstream length of 1.06 cm ($15L_D$) for these conditions. The appropriate radial extension for the probe geometry is not so neatly provided, and is set to one quarter-radius beyond the probe edge. Previous experience with the computational code suggests that the maximum cell spacing should be at least a factor of 12 smaller than the Debye length. Rounding in favor of conservative values, the cells are dimensioned at 4×10^{-5} m on a side. The final geometry extends 390 cells (1.560 cm) along the probe axis and 390 cells (1.560 cm) radially, with 238 elements (0.952 cm) along the collecting surface and 80 elements (0.320 cm) along the guard ring. Altogether there are 112,350 cells outside of the probe body. Dimensions of the probe front face are selected to match the experimental instrument in Ref. 10.

The simulation time step is selected so that the fastest ions travel less than one cell length per iteration. For the beam populations, ions that enter at twice the thermal speed beyond the drift velocity arrive at the probe with a velocity of 6,220 m/s. Dividing the cell length by this speed and rounding down sets the time step at 5×10^{-9} s.

Each probe simulation is run for 20,000 iterations to reach a steady state, followed by 40,000 sampled iterations. At steady state the simulations include 1.2 to 1.5 million particles. A simulation can be completed in 25 hours when run on a 3.8 GHz Pentium 4 system.

A. Single Beam Population

Contour plots of the flow field (Figs. 7-9) show curvature at the outer radial edge of the probe. The guard ring appears to operate as desired however, since potential contours upstream of the collecting surface are parallel. The outermost edge of the domain may be too close to the probe, as evidenced by the significant change in curvature of the contours beyond $r = 0.014$ m. The effect seems to be localized to the outermost 1 mm, but additional simulations on an extended domain are needed to confirm that surface properties are unaffected. The radial sheath is likely to be larger than the axial due to the lower transverse velocity.

Plasma properties over the first 100 cells (4 mm) at a fixed axial position are combined into radial-average profiles of the sheath. These profiles show very good agreement with Bohm sheath solution profiles of potential,

electron density, and ion density for the single beam distribution (Figs. 10-12). The potential and electron density are related through the Boltzmann relation, so any fluctuations in the potential profile are magnified in the electron density profile. The simulated ion profile consistently falls approximately 5% lower than the Bohm sheath profile near the probe, which is due primarily to the non-zero ion temperature.

B. Composite Beam and CEX Population

The composite distribution is the linear superposition of two Maxwellian distributions. Although the two components are unlikely to interact through collisions, collective effects will provide some coupling. In order to quantify such effects, both of the component distributions are first simulated separately. The full composite distribution is then simulated with both components together. This has the additional benefit of using a third more particles than the single beam distribution, giving slightly better statistics. Contour plots of the potential, electron density, and ion density for the composite distribution (Figs. 13-15) show the same features as the single beam flow field, but with a smaller scale sheath. This reduced scaling is expected from the higher total ion density and correspondingly smaller Debye length.

Figures 16 and 17, respectively, show the normalized change in density from separate to composite simulations for the beam and CEX populations. Interestingly, both populations show a 10 to 15% density increase a few millimeters upstream of the probe surface, but remain unchanged elsewhere. Physically, the increased charge density due to the additional component is more effective at shielding the bulk of the plasma from the potential drop near the surface. However, plasma moving through the sheath still sees the full potential drop and so must reach the same final velocity. Recalling that conservation of mass is equivalent to conservation of flux in this setting, the same final density must also be reached at the surface.

Radial-average profiles are calculated for the composite distribution as described in the single beam case. For comparison, a Bohm sheath solution is calculated using the “composite bulk” properties in Table 1. The temperature is not well-defined for this distribution, but is not required for the solution. As seen in Figs. 18-20, the simulated profiles prove to be in remarkably good agreement with this approach. The difference between the simulation and Bohm sheath ion density profiles remains at the 5% magnitude expected on the basis of a non-zero ion temperature.

V. Effects of Guard Ring Bias

It is standard experimental practice to bias the entire Faraday probe to a single potential. The desired result is a uniform sheath over the front of the probe so that current is not preferentially focused onto the collector. In a numerical simulation, current streamlines can be traced to identify conditions where such focusing occurs.

The single beam and composite simulations are repeated for a range of guard ring biases from 0 V to -10 V. The collecting area is held constant at -5 V so that the base ion current remains unchanged. One data point is immediately available from the previous simulations: the standard case of a probe held at a uniform potential. Macroscopic current streamlines are then traced for several positions along the inlet of the domain. When operating with a uniform sheath as desired, streamlines that terminate on the collecting surface will be purely axial. Curvature toward or away from the axis indicates collection of too much or too little current.

Limiting cases are presented for the single beam case in Figs. 21-23. The uniform bias condition has streamlines that are straight to within the numerical scatter of the simulation, indicating that the standard practice is entirely appropriate. Even at ± 5 V, the streamlines show less than 0.3 mm of radial deflection. However, plotting the collected current versus guard ring bias as in Fig. 24 demonstrates a more noticeable impact of 0.5 μ A or about 4% of the collected ion current.

The composite distribution is more susceptible to focusing, since it has a larger fraction of ions at lower velocities. The uniformly biased condition is still virtually ideal, but the limiting cases show streamline deflections approaching 0.5 mm (Figs. 25-27). The error induced in the collected ion current also scales more strongly with the guard ring bias as seen in Fig. 28. A ± 5 V variation results in a 1.2 μ A or 10% change in collected ion current.

VI. Langmuir Probe Mode

The generality of the Langmuir probe technique makes it possible to operate a Faraday probe in a Langmuir probe mode. That is, recording collected current during a sweep of bias voltage provides essentially the same current versus voltage or “IV” characteristic as a traditional wire Langmuir probe. Ion and electron currents are collected simultaneously, and analysis of the characteristic will ultimately resolve them.

One possible difficulty could arise if the Faraday probe focuses current onto the collecting surface at some voltages. This would distort the IV characteristic and likely render subsequent analysis worthless. Fortunately, as

demonstrated in the previous section, even a small focusing of current streamlines results in a relatively large change in collected current. Abrupt changes in collected current indicate that the probe is not operating as expected.

The single beam and composite simulations are repeated again for a range of uniform probe biases from -10 V to 0 V. A complete Langmuir probe trace would continue to positive bias in order to identify an electron saturation current. The physics involved in that limit are not consistent with the Boltzmann relation, which incorrectly predicts an unlimited exponential increase in electron density. Rather than analyze each flow field to determine whether the current streamlines are being focused, the collected currents are compiled directly into a partial IV characteristic.

The single beam and composite distribution characteristics are shown respectively in Figs. 29 and 30. Both characteristics show a near-constant current at large negative potential, corresponding to the ion saturation current. At smaller potential, such that $\phi_w < T_e$, the electron current dominates over the ion current and drives an exponential increase in collected current. Simulated currents are typically within 0.1 μA of the theoretical values as calculated from freestream flux (for ions), or detailed continuity (for electrons). This uniformly excellent agreement indicates that the probe should be reliable for current measurements over the full range from -10 V to 0 V.

VII. Conclusion

A hybrid PIC code was used to simulate axisymmetric plasma flow near a Faraday probe. Two ion distributions were used; the first was a simple Maxwellian beam ion distribution and the second was a superposition of beam and CEX ion distributions, representing a low-power Hall thruster plume. The planar Bohm sheath solution was found to be a reliable predictor in all simulations for plasma potential, ion number density, electron number density, and collected current at the probe surface.

Effects of varying the guard ring bias from the collecting surface bias were quantified in terms of the macroscopic current streamlines and collected ion current. The sensitivity of the collected current to any focusing in the flow field made it possible to simulate the negative bias branch of a Langmuir probe characteristic. Simulated currents very accurately reproduced both ion and electron currents over the range -10 V to 0 V.

The implication of this universal agreement between the Bohm sheath theory and simulation results is that the Faraday probe is a robust instrument over a range of bias potentials and operating conditions. Collected current is not sensitive to the ion distribution, provided the guard ring extends sufficiently far from the collecting surface. If the guard ring were significantly thinner, edge effects would overrun the planar region and the flow field would deviate from the Bohm sheath solution.

Acknowledgments

Support for this work is provided by the Jet Propulsion Laboratory with Lee Johnson as the technical monitor. The authors also thank Tammy Ma and David Conroy for sharing their experimental data.

References

- ¹Fife, J. M., Hargus, W. A., *et al.*, "Spacecraft Interaction Test Results of the High Performance Hall System SPT-140," AIAA-2000-3521, 36th AIAA/ASME/SAE/ASEE Joint Propulsion Conference, Huntsville, AL, July 20-23, 2000.
- ²Hofer, R. R., Hass, J. M., Gallimore, A. D., "Ion Voltage Diagnostics in the Far-field Plume of a High Specific Impulse Hall Thruster," AIAA-2003-4556, 39th AIAA Joint Propulsion Conference, Huntsville, Alabama, July 20-23, 2003.
- ³King, L. B., Gallimore, A. D., Maresse, C. M., "Transport-Property Measurements in the Plume of an SPT-100 Hall Thruster," *Journal of Propulsion and Power*, Vol. 14, No. 3, May-June 1998, pp. 327-335.
- ⁴Lieberman, M., Lichtenberg, A., *Principles of Plasma Discharges and Materials Processing*, John Wiley & Sons, New York, NY, 1994, pp. 154-160.
- ⁵Chen, Francis, *Introduction to Plasma Physics and Controlled Fusion, Vol. 1*, Plenum Press, New York, NY, 1984.
- ⁶Birdsall, C. K. and Langdon, A. B., *Plasma Physics Via Computer Simulation*, Adam Hilger Press, 1991.
- ⁷Bird, G. A., *Molecular Gas Dynamics and the Direct Simulation of Gas Flows*, No. 42 in Oxford Engineering Science Series, Oxford University Press, 1994.
- ⁸Boerner, J., Boyd, I. D., "Numerical Simulation of Probe Measurements in Non-equilibrium Plasma," AIAA-2005-4790, presented at 36th AIAA Plasmadynamics and Lasers Conference, Toronto, ON, Canada, June 6-9, 2005.
- ⁹Boyd, I. D. and Yim, J. T., "Modeling of the Near Field Plume of a Hall Thruster," *Journal of Applied Physics*, Vol. 95, 2004, pp. 4575-4584.
- ¹⁰Ma, Tammy, "Quantification with Two-Dimensional Spatial Resolution of the Ion Flux Emitted from a 200 W Hall Effect Thruster," California Institute of Technology, Pasadena, California, 2004, (unpublished).
- ¹¹deGrys, K. H., Tilley, D. L., Aadland, R. S., "BPT Hall Thruster Plume Characteristics," AIAA-99-2283, 36th AIAA Joint Propulsion Conference, Los Angeles, CA, June 20-24, 1999.

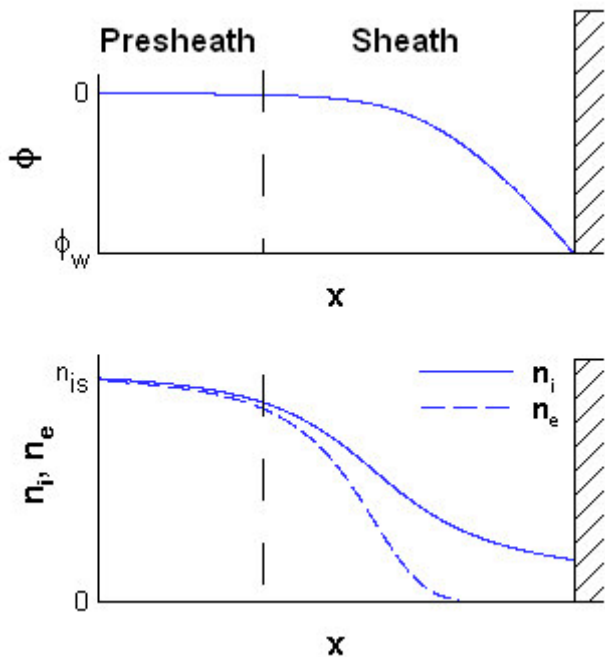


Figure 1. Schematic planar sheath structure.

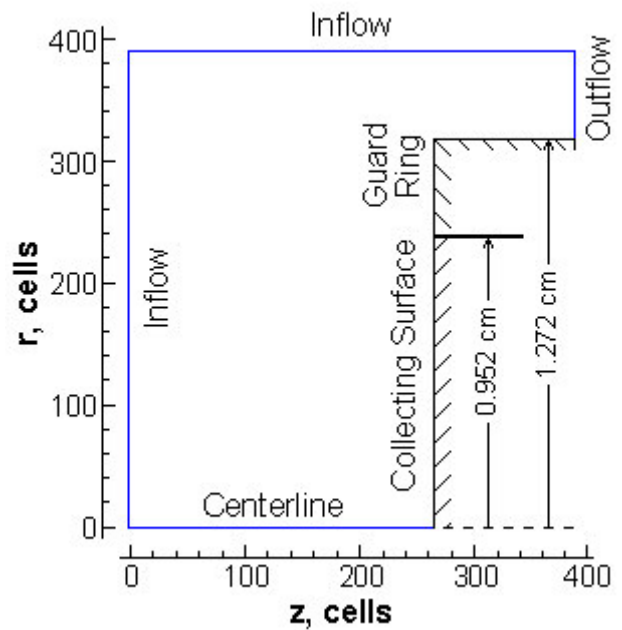


Figure 2. Computational domain, with probe surfaces at the right lower corner.

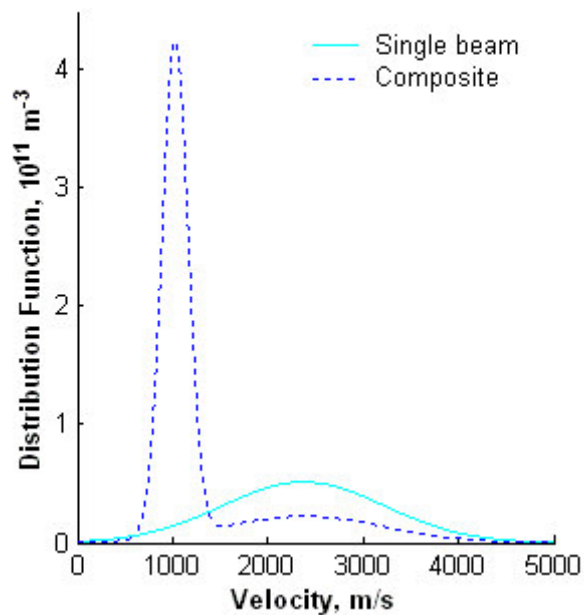


Figure 3. Velocity distributions for single beam and composite distributions. The large fraction of CEX ions is especially prominent.

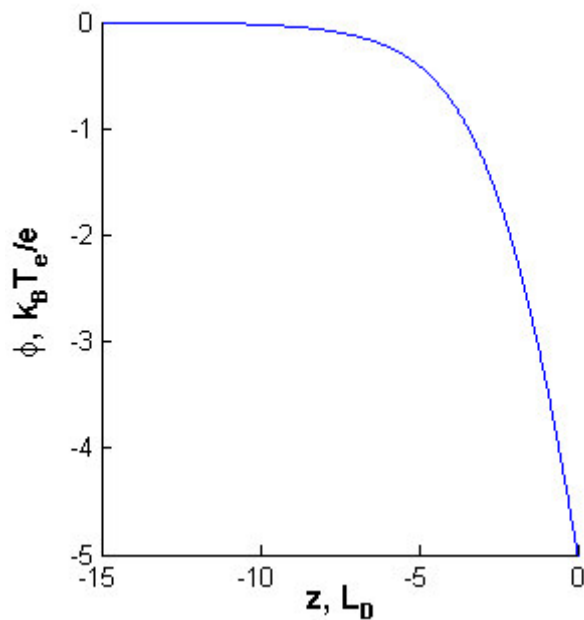


Figure 4. Bohm sheath potential profile for composite CEX ions and an applied surface potential $\phi_w = -5$ V.

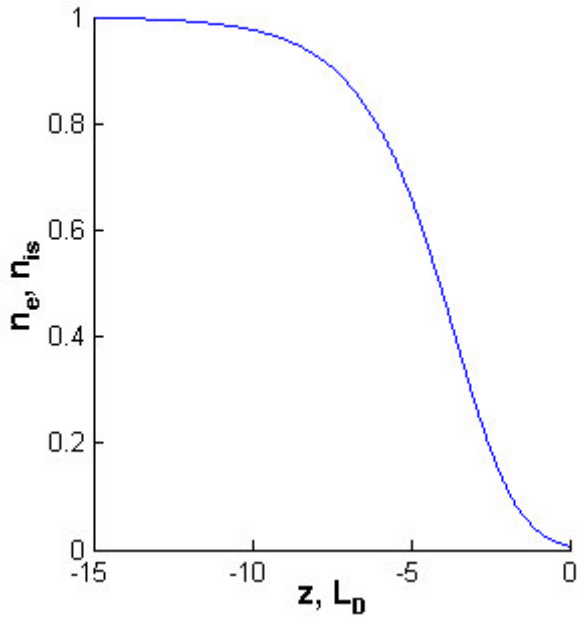


Figure 5. The Bohm sheath electron density profile for composite CEX ions shows deviation beyond $12L_D$.

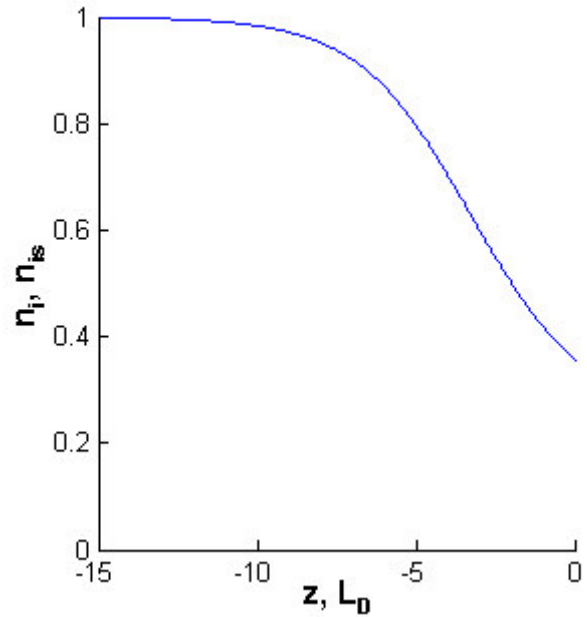


Figure 6. Bohm sheath ion number density profile for composite CEX ions.

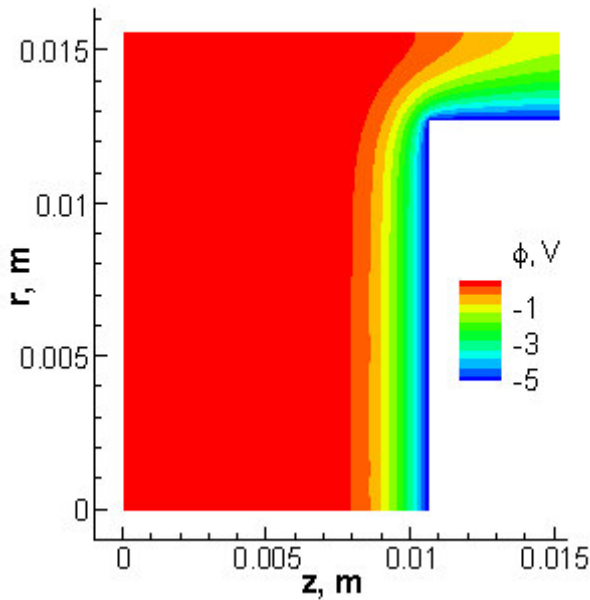


Figure 7. Simulated potential contours for the single beam distribution. The potential remains nearly planar over the entire collecting surface.

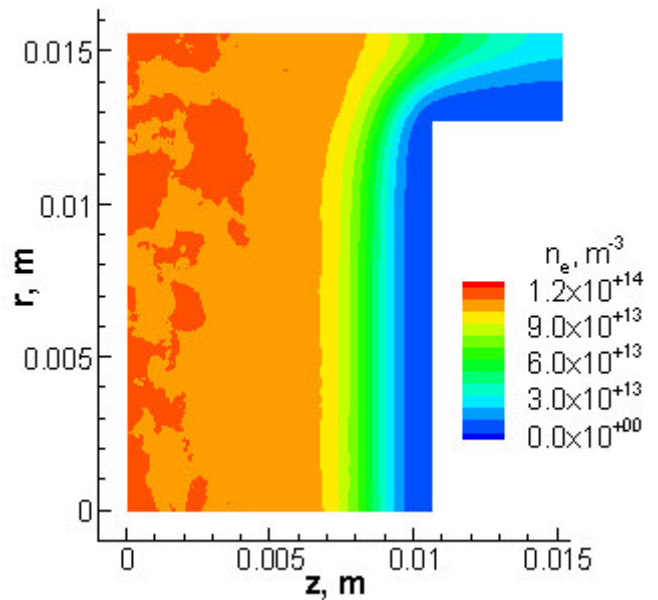


Figure 8. Simulated electron density contours for the single beam distribution, with small variations accentuated by the Boltzmann relation.

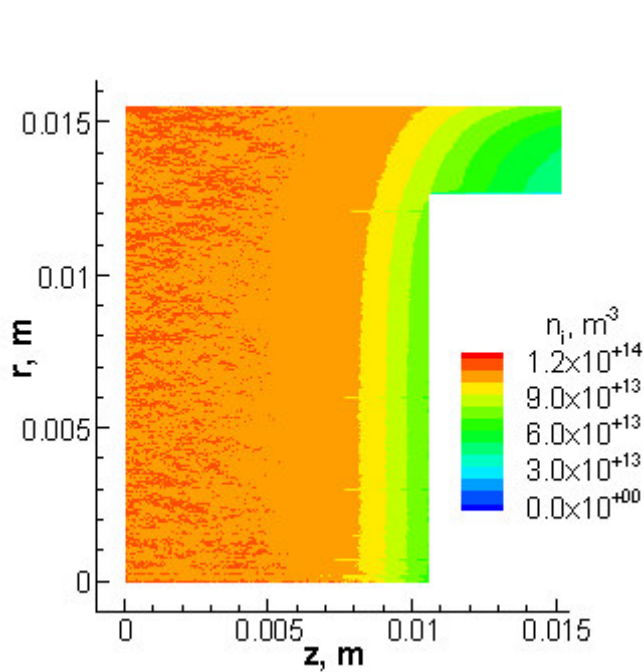


Figure 9. Simulated ion density contours for the single beam distribution.

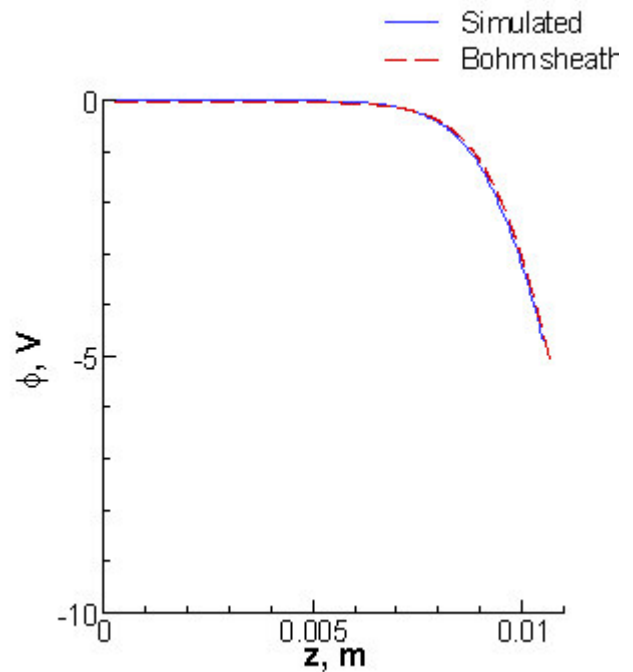


Figure 10. Radial-average simulated potential agrees extremely well with the Bohm sheath solution.

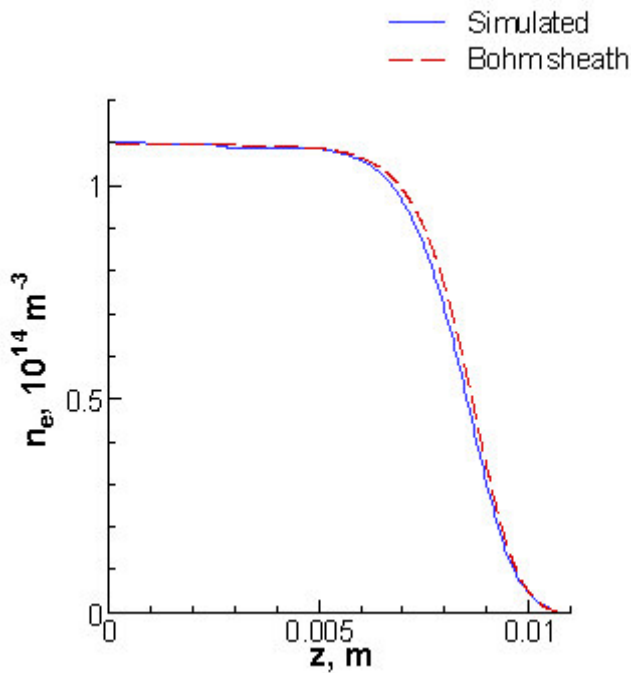


Figure 11. Discrepancies between the Bohm sheath solution and the potential are magnified in the electron density profile.

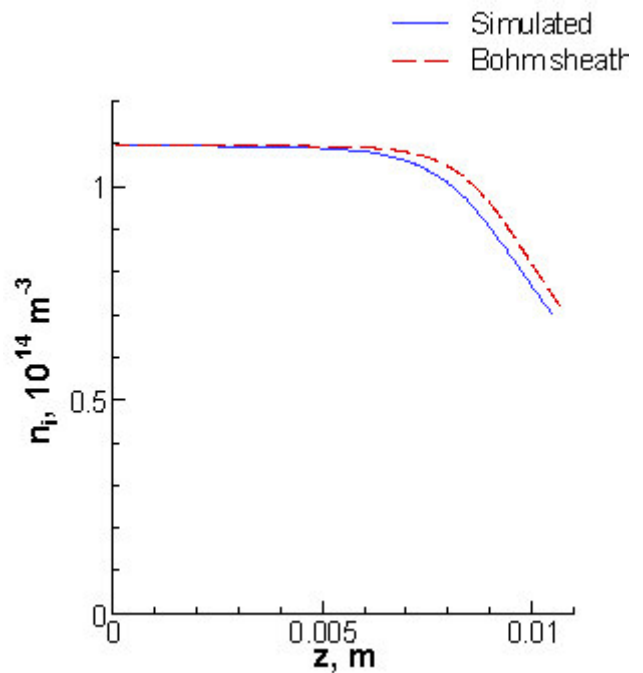


Figure 12. Due to non-zero ion temperature, the simulated ion density near the probe is slightly lower than the Bohm sheath solution predicts.

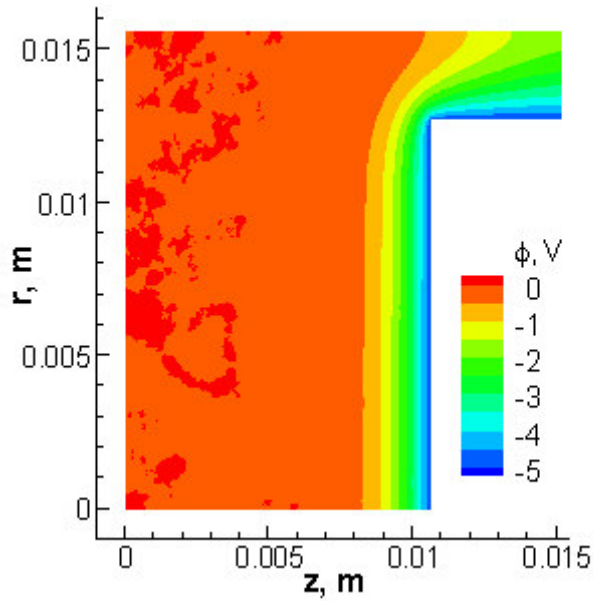


Figure 13. Simulated potential contours for the composite distribution. Note that the sheath is compressed compared to the single beam case, Fig 7.

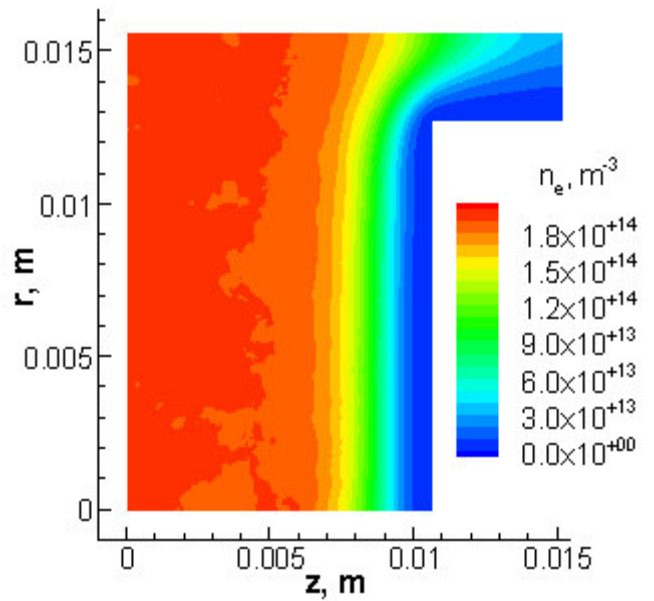


Figure 14. Simulated electron density contours for the composite distribution.

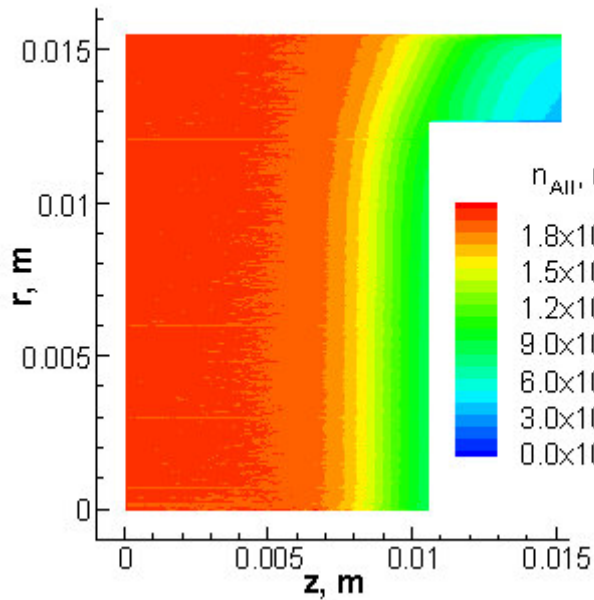


Figure 15. Simulated ion density contours for the composite distribution.

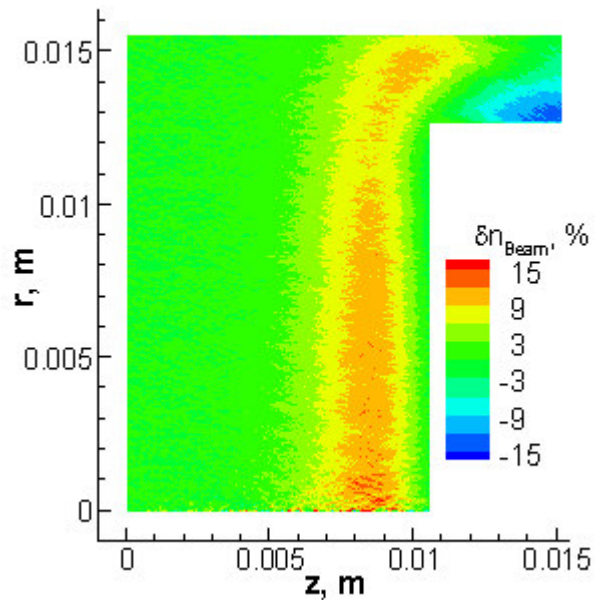


Figure 16. Normalized difference in beam ion density between separate and composite simulations.

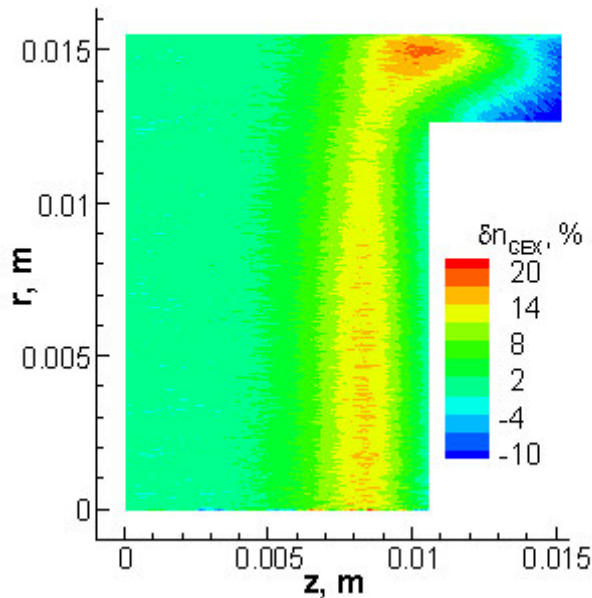


Figure 17. Normalized difference in CEX ion density between separate and composite simulations. Note the scale change from the previous figure—both population densities rise 10 to 15% away from the surface.

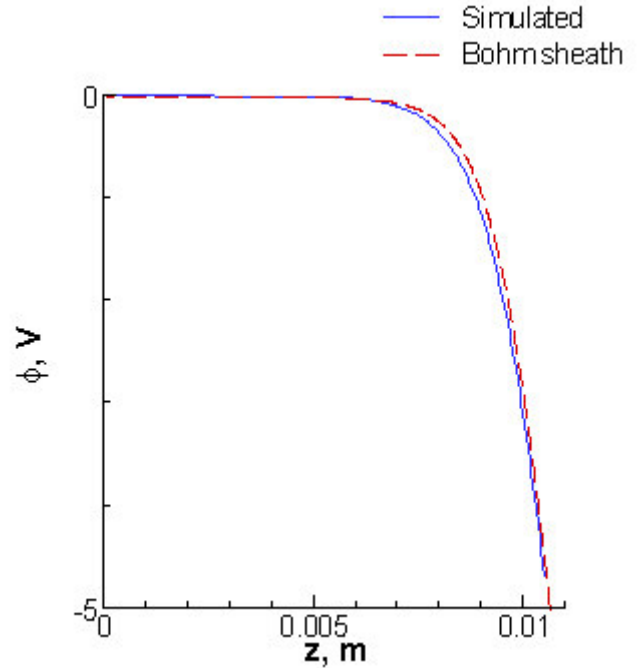


Figure 18. The radial-average simulated potential for the composite distribution remains in good agreement with the Bohm sheath solution.

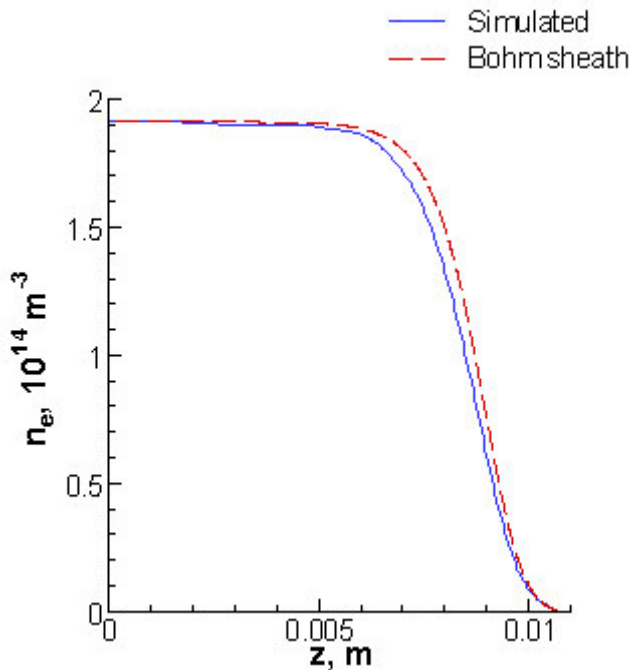


Figure 19. Radial-average simulated electron density for the composite distribution.

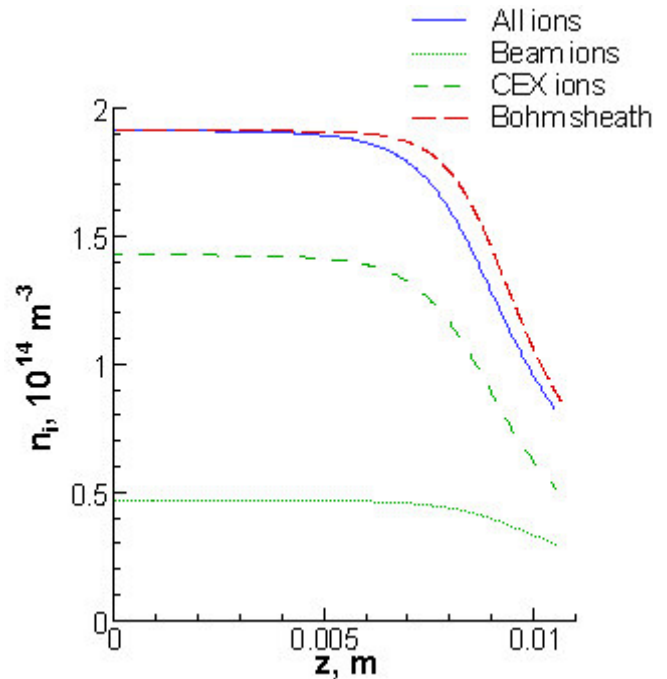


Figure 20. The bulk property solution models the composite ion density surprisingly well. The error level remains consistent with a non-zero ion temperature.

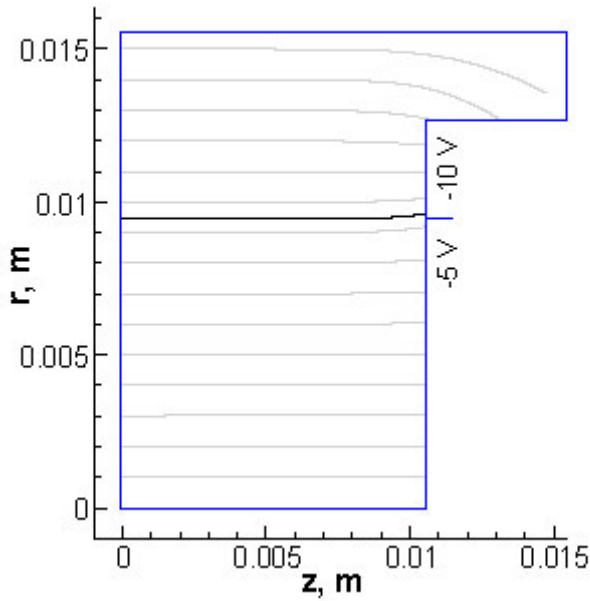


Figure 21. Mean current flow streamlines for single beam ions with stronger guard ring potential.

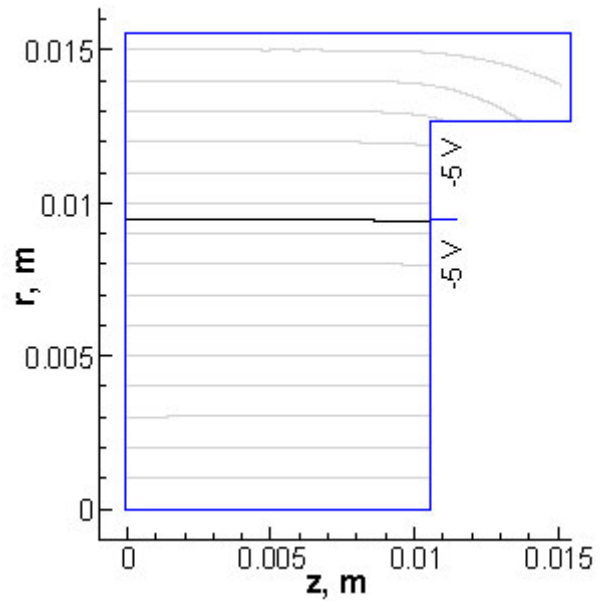


Figure 22. The mean current flow streamlines for single beam ions indicate negligible focusing of ion current at a uniform probe potential.

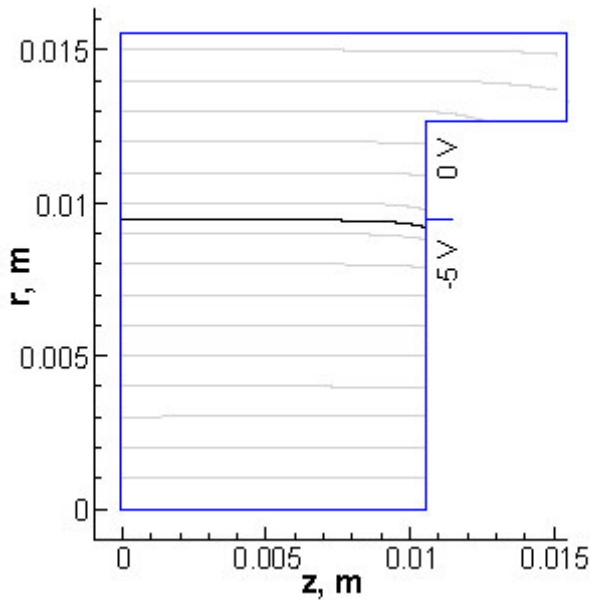


Figure 23. Mean current flow streamlines for single beam ions with weaker guard ring potential.

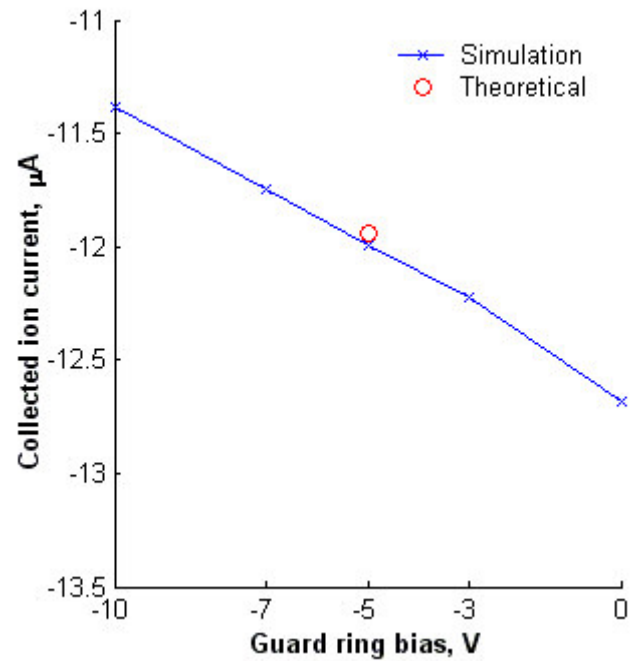


Figure 24. Collected ion current varies almost linearly with guard ring bias.

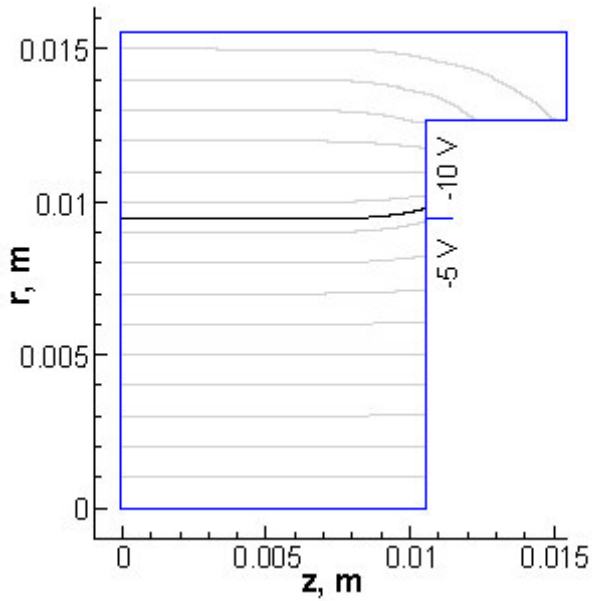


Figure 25. Mean flow streamlines for composite ions with stronger guard ring potential.

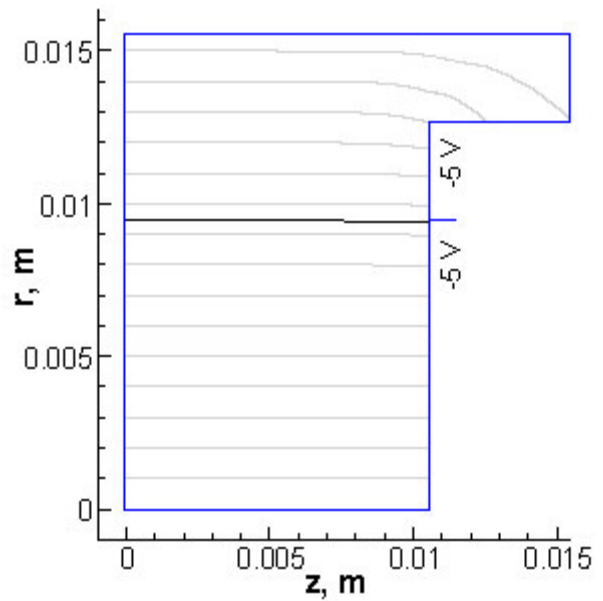


Figure 26. The mean flow streamlines for composite ions indicate negligible focusing of ion current for a uniform probe potential.

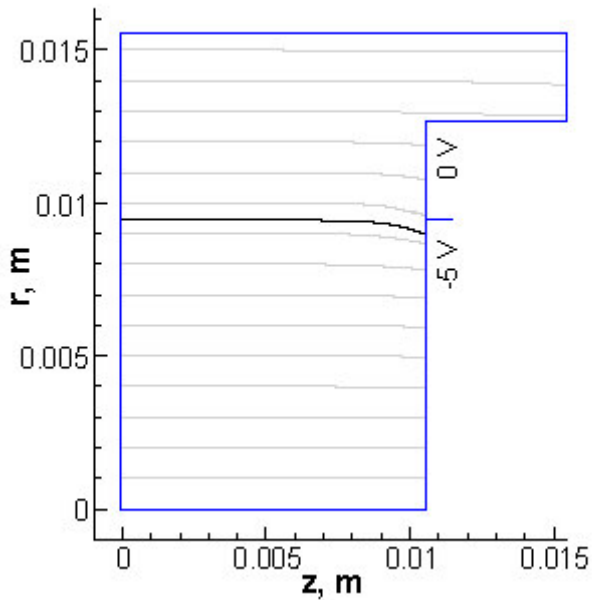


Figure 27. Mean flow streamlines for composite ions with weaker guard ring potential.

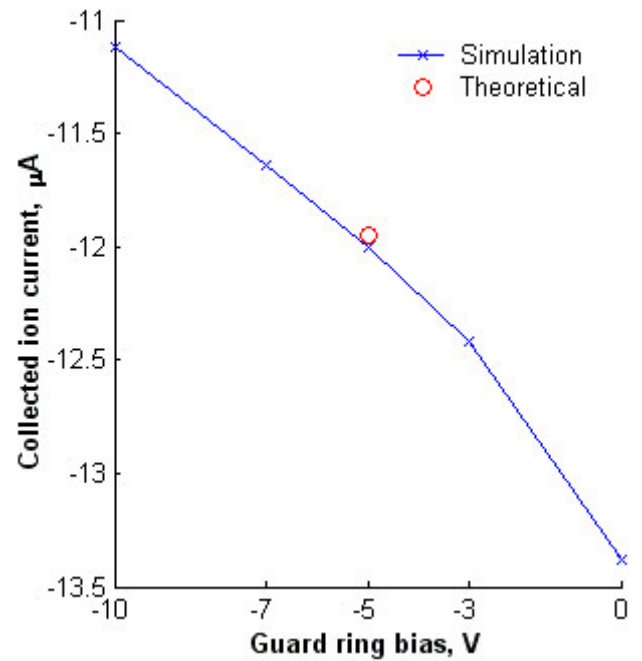


Figure 28. Collected current still varies almost linearly with guard ring bias, but with a stronger correlation for the composite distribution.

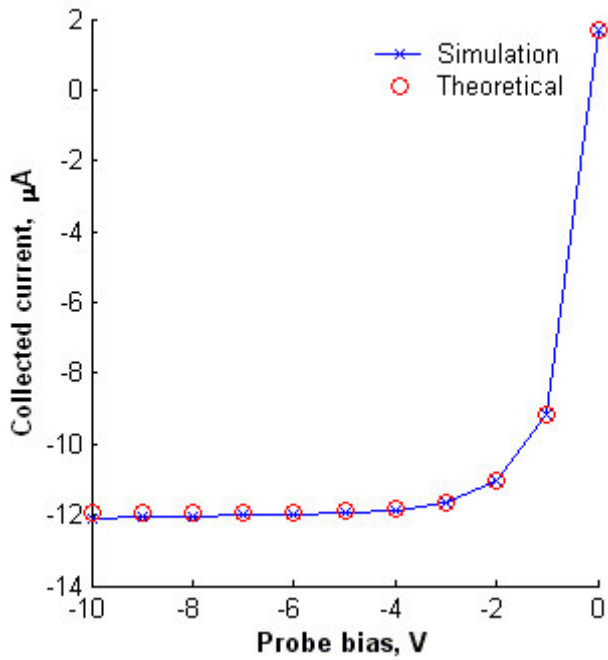


Figure 29. The simulated IV characteristic for a single beam distribution is in excellent agreement with theory.

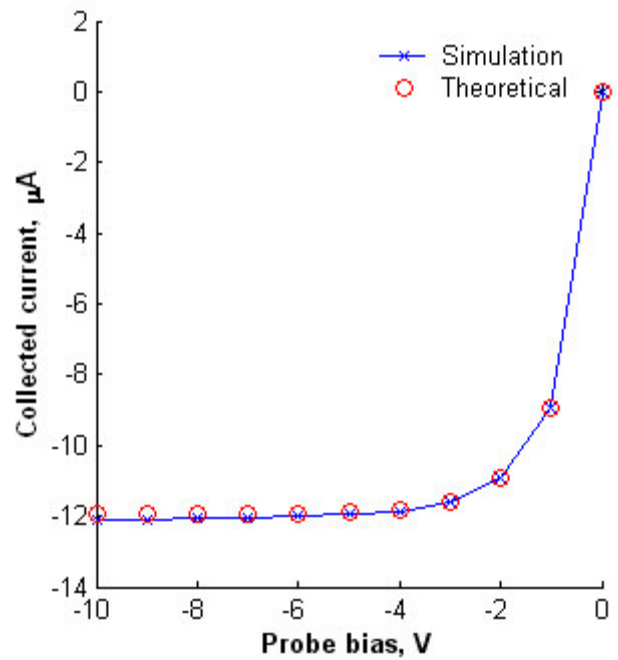


Figure 30. The simulated IV characteristic for the composite distribution suggests reliable probe operation over the entire ion-collecting region.